RSC Advances

PAPER

View Article Online
View Journal | View Issue

Cite this: *RSC Adv.*, 2020, **10**, 15769

Raspberry-like Pd_3Pb alloy nanoparticles: superior electrocatalytic activity for ethylene glycol and glycerol oxidation†

Yujie Duan,[a] Zhelin Liu,[a] Bo Zhao *[ab] and Jinghai Liu[b]

Received 18th January 2020
Accepted 11th April 2020

DOI: 10.1039/d0ra00564a

rsc.li/rsc-advances

Pd_3Pb catalysts are one of the state-of-the-art catalysts for the electrooxidation of alcohols. Herein, raspberry-like Pd_3Pb catalysts are synthesized *via* a simple method. The materials are characterized using various physical techniques. The electrocatalytic behaviors of the products towards the oxidation of ethylene glycol and glycerol are investigated. Electrochemical results show that the raspberry-like Pd_3Pb nanostructure produces excellent electrocatalytic activity and stability towards the electrooxidation of ethylene glycol and glycerol in alkaline media, which endows the prepared nanostructure with promising potential in applications like fuel cells.

Introduction

With the development of society and the economy, more and more non-renewable energies are facing depletion due to excessive exploitation and utilization. Meanwhile, environmental pollution and global warming triggered by fossil fuel consumption have become the bottleneck impeding the development of society.[1] Thus, it is especially important to explore renewable energies to protect the environment and human health from the harm brought by the burning of fossil fuels. Fuel cells have attracted extensive interest owing to their great merits including high efficiency and cleanness.[2,3] Direct alcohol fuel cells (DAFCs), possessing high efficiency in energy conversion process with wide variety of sources, have received widespread concerns in recent years. What is more, DAFCs also own the advantages of low environmental pollution and easy transportation.[4] One important factor affecting the ultimate performance is the reaction on the anode of DAFCs, the oxidation of organic molecule like methanol. Therefore, more and more attention has been paid to the electrooxidation of methanol,[5,6] ethanol,[7] long-chain ethylene glycol and glycerol.[8]

Noble metal nanomaterials possess great potentials as practical candidates for future power supply.[9] As the most promising candidate of anode catalysts for alcohol oxidation, Pt has been widely studied due to its superior electrocatalytic efficiency.[10] Thus, Pt and Pt-based nanomaterials have been applied in many fields, such as fuel cells and biosensors owing to their high catalytic activity and stability.[11] However, several disadvantages have hindered the commercial application of Pt catalysts, such as rare reservation, high cost and poor stability.[12] Therefore, many approaches have been developed for the fabrication of Pt-based nanomaterials. Since the electrocatalytic property of Pt-based nanomaterials can be tuned by manipulating the precursors, reaction conditions and preparation methods, one promising strategy to improve the electrochemical performance is alloying Pt with a second transition metal which holds advantages comparing with monometallic catalysts owing to the existence of synergistic effect between the two metals. A series of measures have been utilized in alloying Pt with Ni,[13,14] Cu,[15] Pd,[16] Fe,[17] and Pb.[18–20] Huang *et al.*[19] successfully prepared platinum–lead concave nanocubes with excellent electrocatalytic performance towards methanol oxidation, which is contributed by the synergistic effect of Pt–Pb alloys. However, it is still a challenge using platinum-based materials in practical DAFCs due to its poor activity and durability under the alkaline condition.[21]

Recently, many strategies have been developed to the fabrication of non-Pt electrocatalysts with both enhanced activity and durability for alcohol oxidation reactions,[22] among which Pd-based electrocatalyst is more likely to be a promising substitute since Pd possesses similar atomic size and crystal structure with Pt. Compared with Pt catalysts, Pd catalysts have received more and more attentions, owing to their lower cost and higher poison resistance for CO-like intermediate species.[23,24] However, the electronic structure of monometallic Pd may alleviate the electron transfer during the electrooxidation process, which may limit the Pd material to achieve practical application in DAFCs.[25,26] Thus, adjusting the electronic structure of palladium can facilitate the electron transfer, which in turn promote the conversion efficiency of fuel cells.[27]

[a]*School of Chemistry & Environmental Engineering, Changchun University of Science and Technology, Changchun, Jilin 130022, P. R. China. E-mail: b.zhao@live.cn; Fax: +86-431-85583459; Tel: +86-431-85583459*

[b]*Inner Mongolia Key Laboratory of Carbon Nanomaterials, College of Chemistry and Chemical Engineering, Nano Innovation Institute, Inner Mongolia University for Nationalities, Tongliao, Inner Mongolia 028000, P. R. China*

† Electronic supplementary information (ESI) available. See DOI: 10.1039/d0ra00564a

Comparing with Pd nanomaterials, Pd-based intermetallic alloy possesses the advantages of optimized catalytic activity, improved CO-resistance ability and enhanced stability. One effective way to form intermetallic alloy is to decorate Pd with other cheaper transition metals, such as Cu,[28] Pb,[29] Ni,[30] and Ag,[31] and uncountable efforts have been devoted into this area. Besides, the shape, morphology, and surface chemistry of Pd material also affect its property for specific applications.[32] Therefore, Pd-based catalysts with different morphologies have been synthesized to enhance the electrocatalytic performance.[33–37] For example, Shi *et al.*[34] fabricated Pd_3Pb nanowire network with excellent electrocatalytic performance, which can be ascribed to the modified electronic structures by incorporating with Pb. Jana *et al.*[35] successfully prepared the flower-like ordered Pd_3Pb nanocrystals which exhibit preferable electrocatalytic activities. Asset *et al.*[37] reported the synthesis of Pd–Pb catalysts by a modified sacrificial support method for glycerol and ethylene glycol electrooxidation. To the best of our knowledge, raspberry Pd_3Pb alloy nanoparticles for electrooxidation of ethylene glycol and glycerol have been rarely reported.

Herein, raspberry-like Pd_3Pb nanocomposites are prepared by a facile one-pot method. The electrocatalytic activity and stability of the as-prepared nanocomposites are systematically examined in alkaline media, which are further compared with commercial 10% Pd/C catalyst.

Experimental

Chemicals

Chemicals including palladium(II) acetylacetonate ($Pd(acac)_2$), lead(II) formate ($Pb(COOH)_2$), citric acid, octadecylene (ODE), ascorbic acid (AA), oleylamine (OAm), ethanol (C_2H_6O), hexadecyltrimethylammonium chloride (CTAC), and cyclohexane (C_6H_{12}) were of analytical grade and used as received without further purification. Ultrapure water (18.2 MΩ cm) was used in all experiments.

Preparation of palladium–lead nanocomposite

In a typical synthesis, 15.2 mg $Pd(acac)_2$, 5.0 mg $Pb(COOH)_2$, 15.5 mg AA, 15.6 mg citric acid, 6.4 mg CTAC, 2.0 mL ODE and 8.0 mL OAm were added into a round-bottom flask. The flask was sealed and ultrasonicated for two hours. The resulting solution was heated to 160 °C under magnetic stirring in an oil bath and kept for six hours. After naturally cooling down to room temperature, the obtained product (Pd_3Pb alloy) was centrifuged, washed several times with a cyclohexane/ethanol (v/v = 1/9) mixture, and redispersed in ethanol for further characterization. Besides that, Pd and palladium–lead nanomaterials with other Pd to Pb ratios of 1 : 1 (PdPb) and 1 : 3 ($PdPb_3$) were also obtained by simply changing the precursor masses. The metal amounts were identified by inductively coupled plasma atomic emission spectrometry (ICP-AES).

Structure, composition and morphological characterizations

Transmission electron microscopy (TEM) and high-resolution TEM (HRTEM) images of the as-prepared palladium–lead alloys were obtained on a Tecnai G2 S-Twin F20 transmission electron microscope. The scanning electron microscopy (SEM) and energy dispersive X-ray spectroscopy (EDX) images of palladium–lead alloys were acquired on XL 30 ESEM-FEG. X-ray diffraction (XRD) measurements were conducted on a D/max 2550 V/PC X-ray diffractometer using Cu (50 kV, 200 mA) radiation. X-ray photoelectron spectroscopy (XPS) test was performed on an ESCALAB-MKII spectrometer. ICP-AES was carried out on OPTIMA 3300DV (PerkinElmer).

Electrochemical measurements

Electrochemical measurements including cyclic voltammetry (CV) and chronoamperometry (CA) were performed on a CHI660E electrochemical workstation (Shanghai Chenhua, China), employing a traditional three-electrode system which includes a glassy carbon electrode (GCE) with a diameter of 3 mm as the working electrode, a Pt wire as the counter electrode and a saturated calomel electrode (SCE) as the reference electrode. GCE was polished to mirror with alumina paste before performing the electrochemical measurements. The modified GCE was fabricated by dropping and drying the as-prepared catalyst ink on GCE surface, which was covered by 10 μL of 0.5 wt% Nafion and then dried in air. CV measurements were performed at room temperature in 1 M KOH aqueous solution in the presence or absence of organic molecules within the potential range from −0.8 to 0.4 V at a scan rate of 50 mV s^{-1}. CA tests were measured in 1 M KOH aqueous solution containing 1 M ethylene glycol or glycerol at applied potentials.

Results and discussion

In this study, raspberry-like palladium–lead alloy nanoparticles were prepared by a simple one-pot method. SEM is firstly employed to examine the morphology of the prepared Pd_3Pb nanomaterial, as shown in Fig. 1A. It can be seen that the as-prepared products show sphere-like structure with rough surfaces in an average diameter of 97 nm. Fig. 1B is the TEM image of the prepared Pd_3Pb alloy, and a raspberry-like nanostructure can be observed for every obtained particle. Besides, raspberry-like surface can also be seen for other palladium–lead alloys (Fig. S1†), indicating the variation of metal precursor amount does not significantly affect the resulting morphology. In this way, Pd_3Pb raspberry-like alloy is further examined as an example in the following studies. As is known, AA and citric acid are both common reducing agent. Since the reducing capability of citric acid is relatively poorer than AA, AA is employed as the primary reducing agent in the preparation of raspberry Pd_3Pb nanoparticle. The roles CTAC and citric acid played in the preparation are also further investigated, and the TEM images of products prepared without CTAC (A) or citric acid (B) are shown in Fig. S2.† It can be observed that when CTAC is absent, irregular particles with poor dispersion appear (Fig. S2A†), while agglomeration is seen for the product when CA is not present in the preparation (Fig. S2B†), suggesting that both CTAC and citric acid are of importance as the stabilizing and

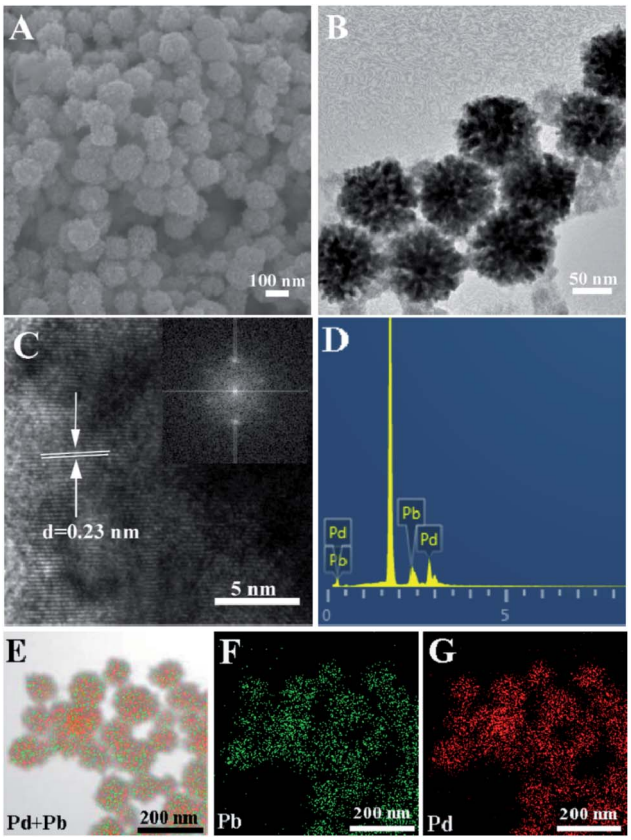

Fig. 1 SEM (A), TEM (B), HRTEM (C), EDX (D) and mapping ((E) TEM + overlay; (F) Pb; (G) Pd) images of the raspberry-like Pd_3Pb alloy nanoparticles. Inset in (C) is the FFT image.

structure-directing agents. TEM results imply that both CTAC and citric acid are important in the formation of raspberry-like Pd_3Pb alloy nanoparticles.

HRTEM is employed to obtain further lattice fringe information of the as-prepared raspberry-like nanoparticles, as shown in Fig. 1C. A well-resolved lattice fringe inter-planar distance of 0.23 nm can be seen, which is ascribed to the lattice spacing distance of Pd_3Pb (111) plane. Besides, the fast Fourier transform (FTT) image of the prepared nanoparticle also corresponds to the Pd_3Pb (111) plane (inset in Fig. 1C). Fig. 1D shows the typical EDX image of the prepared nanoparticle, which reveals the presence of Pd and Pb in the composite. Besides, the atomic ratios of Pd to Pb ratio for Pd_3Pb, PdPb, and $PdPb_3$ are confirmed to be 3 : 1, 1 : 1, and 3 : 1, respectively. EDX elemental mapping is further utilized to show the distribution of Pd and Pb in the prepared nanoparticles. A TEM image is randomly chosen as the mapping area (Fig. 1E), and Pd and Pb elements (Fig. 1F and G) are observed to be evenly distributed on the raspberry-like nanoparticle surface, suggesting the alloy nature.

The crystal structures of the as-prepared Pd_3Pb alloy are further analyzed by XRD technique. As shown in Fig. 2A, diffraction peaks on curve a can be ascribed to the fcc phase of metallic palladium according to JCPDS no. 46-1043. For Pd_3Pb alloy (curve b), the diffraction peaks at 38.6°, 44.8°, 65.3° and

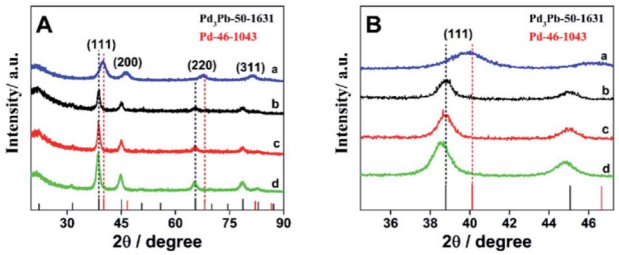

Fig. 2 (A) Comparison of the X-ray diffraction profiles of Pd (a), Pd_3Pb (b), PdPb (c) and $PdPb_3$ (d). (B) Magnified presentation of typical (111) peaks.

78.5° are assigned to the (111), (200), (220) and (311) facets of fcc Pd_3Pb,[35] which in accordance with Pd_3Pb (JCPDS no. 50-1631), further revealing the formation of Pd_3Pb alloy employing the applied method. With the increase of Pb amount, no obvious change can be observed for the crystalline structure (curve c and d). The (111) plane area for the four investigated nanomaterials are magnified, as shown in Fig. 2B. It can be seen that only slight negative shifts are found as the Pb quantity increases.

The valence state and surface composition of the as-prepared raspberry-like Pd_3Pb nanoparticles are revealed by XPS. As illustrated in Fig. 3A, Pb 4f region of the XPS spectrum can be deconvoluted into two pairs of asymmetric peaks. The stronger peaks at binding energies of 136.5 eV and 141.5 eV are ascribed to $4f_{7/2}$ and $4f_{5/2}$ orbitals of metallic lead Pb(0),[36] while the weaker peaks at binding energies of 138.0 eV and 142.6 eV can be assigned to the $4f_{7/2}$ and $4f_{5/2}$ orbitals of PbO(II), which are probably derived from the partial oxidation of Pb on Pd_3Pb surface.[38] Fig. 3B is the Pd 3d XPS spectrum of the prepared nanocomposite, and the peaks of binding energies at 335.3 eV and 340.5 eV are in good consistence with $3d_{5/2}$ and $3d_{3/2}$ orbitals of Pd^0, indicating Pd element mainly exists as zero valence state on the surface of Pd_3Pb nanoparticles. The above analysis results show that metal precursors are efficiently reduced, suggesting the successful fabrication of raspberry-like Pd_3Pb alloy nanoparticles.

It has been reported that Pd-based nanomaterials exhibit good electrocatalytic property towards alcohol oxidation in alkaline media.[24] Therefore, the as-prepared raspberry-like nanoparticles are modified onto the GCE surface to examine the electrochemical behaviors in a typical three-electrode

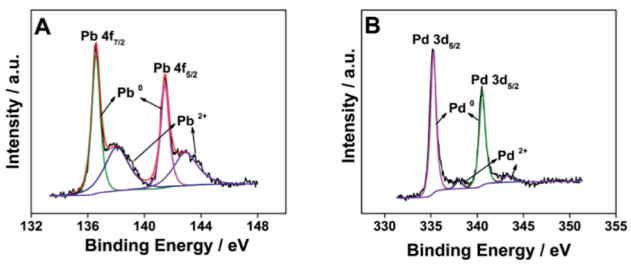

Fig. 3 Pb 4f (A) and Pd 3d (B) regions of the XPS spectrum of the prepared raspberry-like Pd_3Pb alloy nanoparticles.

system. Fig. S3† shows the CV curves of Pd_3Pb (a), PdPb (b), Pd (c), and $PdPb_3$ (d) nanoparticles in 1 M KOH aqueous solution at the scan rate of 50 mV s^{-1}. As depicted in Fig. S3,† reduction peaks characteristic of Pd can be seen on all curves, indicating the successful preparation of Pd during the preparation process. Moreover, raspberry-like Pd_3Pb alloy nanoparticle exhibits the largest electrochemical active surface area (EASA) values in comparison with the other three nanomaterials, showing the possible better performance in the following electrocatalytic investigation.

In recent years, polyols have received much attention as fuel owing to the characteristics like high boiling point, high energy density and renewable ability.[39] Ethylene glycol is one important polyol with a series of merits, such as wide variety of sources, low vapor pressure as well as low toxicity.[40] A great many efforts have been made into the investigation of nanomaterials as catalyst towards the electrooxidation of ethylene glycol.[8,37,41] However, one limitation hinders the applicability of ethylene glycol as a fuel is lacking anode catalyst with high performance for efficient oxidation. Herein, the electrocatalytic performance of the as-prepared raspberry nanoalloy is firstly studied in 1 M KOH aqueous solution containing 1 M ethylene glycol at a scan rate of 50 mV s^{-1} in room temperature, and the corresponding CV curves are shown in Fig. 4A. It can be observed on all CV curves that a strong oxidation peak appears during the forward sweeping process, which can be assigned to the oxidation of ethylene glycol, while another oxidation peak appears on the reverse scan, which corresponds to the removal of incompletely oxidized carbonaceous residues (*e.g.* CO).[42] In addition, raspberry Pd_3Pb nanoalloy exhibits the largest Pd mass activity comparing with the other three products. Histograms of Pd mass activities for different catalysts are pictured in Fig. 4B in order to quantitatively make the comparison. Specifically, the maximum Pd mass activity for Pd_3Pb is 916.1 mA mg_{Pd}^{-1}, which is *ca.* 1.4, 2.6 and 3.8 times of that for PdPb (652.1 mA mg_{Pd}^{-1}), Pd (347.3 mA mg_{Pd}^{-1}) and $PdPb_3$ (243.4 mA mg_{Pd}^{-1}), respectively. Furthermore, the durability of the products are further investigated by CA measurement towards the oxidation of ethylene glycol. Fig. 4C shows the CA curves of Pd_3Pb (a), PdPb (b), Pd (c), and $PdPb_3$ (d) nanomaterials modified GCE in 1 M KOH solution containing 1 M ethylene glycol at the applied potential of −0.12 V. As shown in Fig. 4C, raspberry-like Pd_3Pb alloy nanoparticle still shows higher catalytic activity after 4000 s duration, meaning the best durability among the investigated materials. Above-mentioned results indicate the superior electrocatalytic activity and long-term stability of the prepared raspberry-like Pd_3Pb alloy. As discussed in TEM and XRD analyses, no significant change is observed in crystalline structure and morphology as the Pd to Pb ratio changes. However, the electrocatalytic performance does varies greatly. This may be ascribed to the stable crystalline structure Pd_3Pb forms in a Pd to Pb ratio of 3 : 1. Though atom defects are resulted when Pd to Pb ratio changes, the electrocatalytic capability is not improved on the other products, while Pd_3Pb with the stable crystalline structure possesses the highest electrocatalytic performance in the investigated materials. In addition, the electrocatalytic performance of raspberry Pd_3Pb alloy nanoparticle is also compared with that for commercial 10% Pd/C catalyst. As depicted in Fig. 4D, raspberry Pd_3Pb nanoalloy exhibits much higher Pd mass activity (inset in Fig. 4D) and better stability than commercial 10% Pd/C catalyst. The maximum Pd mass activity of Pd_3Pb is *ca.* 4.2 times of that obtained on the commercial 10% Pd/C catalyst (219.2 mA mg_{Pd}^{-1}), as shown in Fig. S4A.† Besides that, the obtained Pd mass activity on Pd_3Pb is also larger than the other Pd-based nanomaterials reported in previous literatures.[37,43] In addition, the total mass activities for raspberry Pd_3Pb alloy nanoparticle and commercial 10% Pd/C catalyst towards the oxidation of ethylene glycol are also compared (Fig. S4A†), and a maximum current density of 546.1 mA mg_{total}^{-1} is obtained on raspberry Pd_3Pb alloy nanoparticle, which is 24.9 times of that for commercial 10% Pd/C catalyst (21.9 mA mg_{total}^{-1}). All the above results illustrate that the raspberry-like Pd_3Pb alloy is a promising material for the electrooxidation of ethylene glycol.

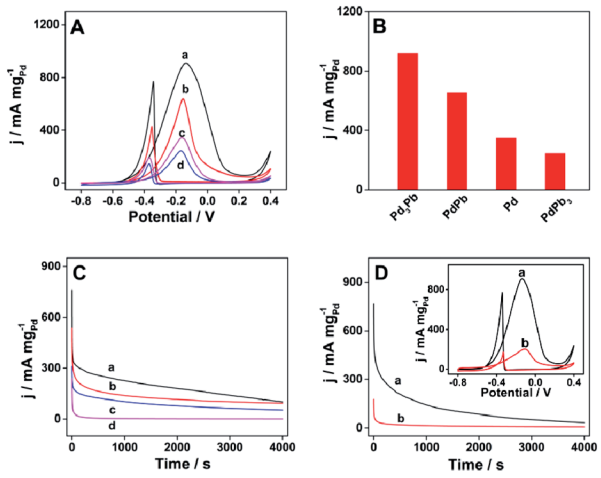

Fig. 4 (A) CV curves of Pd_3Pb (a), PdPb (b), Pd (c) and $PdPb_3$ (d) nanomaterials modified GCEs at the scan rate of 50 mV s^{-1}. (B) Histogram of Pd mass activities for different catalysts towards the electrooxidation of ethylene glycol. (C) CA curves of Pd_3Pb (a), PdPb (b), Pd (c) and $PdPb_3$ (d) modified GCEs at the potential of −0.12 V. (D) CA curves of Pd_3Pb alloy (a) and commercial 10% Pd/C catalyst (b) modified GCEs at the applied potential of −0.12 V. Inset is the CV curves of Pd_3Pb (a) and commercial 10% Pd/C catalyst (b) at the scan rate of 50 mV s^{-1}. Experiments are performed in 1 M KOH aqueous solution and 1 M ethylene glycol.

Glycerol is another polyol developed as fuel for DAFC application.[44] Therefore, the electrocatalytic properties of the prepared materials are further explored in 1 M KOH aqueous solution containing 1 M glycerol. Fig. 5A shows the CV curves of different catalysts towards the electrooxidation of glycerol at the scan rate of 50 mV s^{-1}, among which raspberry-like Pd_3Pb alloy nanoparticle also exhibits the highest Pd mass activity. The maximum Pd mass activities for different catalysts are pictured as histogram in Fig. 5B. Specifically, raspberry-like Pd_3Pb alloy nanoparticle shows a Pd mass activity of 572.8 mA mg_{Pd}^{-1}, which is much higher than PdPb alloy (463.6 mA mg_{Pd}^{-1}), $PdPb_3$ alloy (164.2 mA mg_{Pd}^{-1}) and Pd nanoparticles (350.0 mA mg_{Pd}^{-1}). Besides that, the stability of the catalysts are evaluated by CA measurement. As shown in Fig. 5C, raspberry-like Pd_3Pb

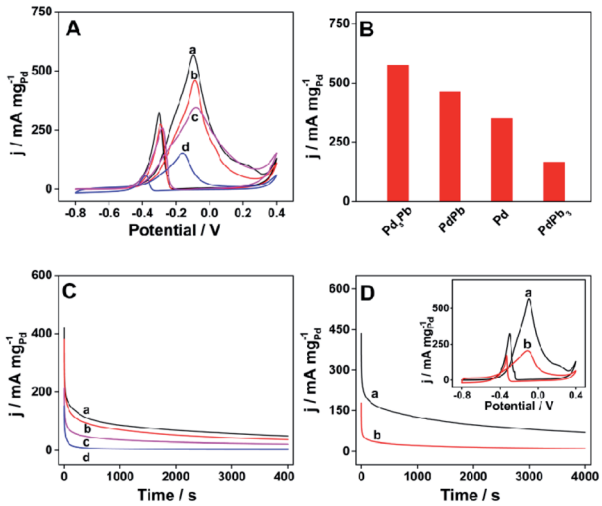

Fig. 5 (A) CV curves of Pd_3Pb (a), PdPb (b), Pd (c) and $PdPb_3$ (d) nanoparticles modified GCEs at the scan rate of 50 mV s^{-1}. (B) Histogram of Pd mass activities on different catalysts towards the electrooxidation of glycerol. (C) CA curves of Pd_3Pb (a), PdPb (b), Pd (c) and $PdPb_3$ (d) modified GCEs at −0.1 V. (D) CA curves of Pd_3Pb alloy (a) and commercial 10% Pd/C catalyst (b) modified GCEs at applied potential of −0.1 V. Inset is the CV curves of the catalysts at the scan rate of 50 mV s^{-1}. Experiments are performed in 1 M KOH aqueous solution containing 1 M glycerol.

alloy nanoparticle still possesses the highest Pd mass activity after 4000 s duration among the four investigated products. In addition, the electrocatalytic performance of the raspberry-like Pd_3Pb alloy is also compared with commercial 10% Pd/C catalyst. Fig. 5D is the CA and CV (inset) comparisons of the two catalysts. As can be seen from Fig. 5D and S4B,† improved electrocatalytic performance including Pd mass activity and stability is found on the raspberry-like Pd_3Pb alloy in comparison with the commercial catalyst towards the electrooxidation of glycerol in alkaline media. What is more, the catalytic activity obtained on Pd_3Pb alloy is also better than some Pd-based nanomaterials previously reported.[37,42] Furthermore, the total mass activities of Pd_3Pb alloy and commercial 10% Pd/C catalyst are further compared, and the corresponding column diagram is shown in Fig. S4B.† The maximum total mass activity for Pd_3Pb can reach 341.4 mA mg_{total}^{-1}, which is 16.4 times of that obtained on the commercial 10% Pd/C catalyst (20.8 mA mg_{total}^{-1}), showing the reduced metal cost in the catalyst utilization. Electrochemical experiments show that the as-prepared raspberry-like Pd_3Pb alloy nanoparticle shows the good electrocatalytic performance towards the oxidation of ethylene glycol and glycerol. The superior electrocatalytic behavior of the raspberry-like Pd_3Pb alloy can be attributed to the following reasons. First, a stable crystalline structure is constructed for the Pd_3Pb alloy. Second, a synergistic effect exists between palladium and lead in the alloy nanoparticles may improve the electrocatalytic activity. Last but not least, the raspberry-like structure may provide more active sites which facilitate the electron transfer.

Conclusions

In this study, Pd_3Pb alloy nanoparticles with a raspberry surface are prepared *via* a simple method and characterized by a series of methods. The roles that citric acid and CTAC played in forming the raspberry-like nanoparticles are investigated. The prepared raspberry Pd_3Pb alloy nanoparticles are employed as electrocatalyst towards the oxidation of ethylene glycol and glycerol in alkaline media. Electrochemical results reveal that the prepared Pd_3Pb alloy shows the best electrocatalytic performance in the investigated three Pd to Pb ratios, which exhibits maximum Pd mass activities of 916.1 mA mg_{Pd}^{-1} and 572.8 mA mg_{Pd}^{-1} for the oxidation of ethylene glycol and glycerol, respectively. Besides, the prepared raspberry Pd_3Pb alloy nanoparticle also shows better electrocatalytic activity and stability than the commercial Pd/C catalyst. The superior electrocatalytic performance for raspberry-like Pd_3Pb alloy may be the contribution of the stable crystalline structure, the raspberry-like surface and the synergistic effect between the two elements.

Conflicts of interest

There are no conflicts to declare.

Acknowledgements

This work is supported by the National Natural Science Foundation of China (21401012, 21501014, 21661026); Scientific and Technological Development Program of Jilin Province (20180520157JH); and Education Department of Jilin Province “13th Five-Year” Science Technology Research Project (JJKH20190557KJ).

References

1 F. Li, X. L. Li, C. Li, J. Shi and Y. Fu, *Green Chem.*, 2018, **20**, 3050–3058.
2 D. Li, K. Cai, L. Wu, Y. P. Zuo, W. M. Yin, H. Zhang, Z. C. Lu, G. L. Zhu and H. Y. Han, *ACS Sustainable Chem. Eng.*, 2017, **5**, 11086–11095.
3 H. You, S. Yang, B. Ding and H. Yang, *Chem. Soc. Rev.*, 2013, **42**, 2880–2904.
4 J. Watt, S. Cheong, M. F. Toney, B. Ingham, J. Cookson, P. T. Bishop and R. D. Tilley, *ACS Nano*, 2010, **4**, 396–402.
5 R. Bavand, Q. Wei, G. Zhang, S. Sun, A. Yelon and E. Sacher, *J. Phys. Chem. C*, 2017, **121**, 23120–23128.
6 J. Sheng, J. Kang, H. Ye, J. Xie, B. Zhao, X. Z. Fu, Y. Yu, R. Sun and C. P. Wong, *J. Mater. Chem. A*, 2018, **6**, 3906–3912.
7 M. Z. Yazdan-Abad, M. Noroozifar, A. R. M. Alam and H. Saravani, *J. Mater. Chem. A*, 2017, **5**, 10244–10249.
8 K. Bhunia, S. Khilari and D. Pradhan, *ACS Sustainable Chem. Eng.*, 2018, **6**, 7769–7778.
9 Y. Xu, X. Cui, S. Wei, Q. Zhang, L. Gu, F. Meng, J. Fan and W. Zheng, *Nano Res.*, 2019, **12**, 1173–1179.
10 H. Ye, Y. Li, J. Chen, J. Sheng, X. Z. Fu, R. Sun and C. P. Wong, *J. Mater. Sci.*, 2018, **53**, 15871–15881.

11 A. C. Chen and P. Holt-Hindle, *Chem. Rev.*, 2010, **110**, 3767–3804.
12 C. He, J. Tao, G. He, P. K. Shen and Y. Qiu, *Catal. Sci. Technol.*, 2016, **6**, 7316–7322.
13 Q. Jiang, L. Jiang, S. Wang, J. Qi and G. Sun, *Catal. Commun.*, 2010, **12**, 67–70.
14 H. Fan, M. Cheng, Z. Wang and R. Wang, *Nano Res.*, 2016, **10**, 187–198.
15 B. A. Lu, T. Sheng, N. Tian, Z. C. Zhang, C. Xiao, Z. M. Cao, H. B. Ma, Z. Y. Zhou and S. G. Sun, *Nano Energy*, 2017, **33**, 65–71.
16 H. Lv, X. Chen, D. Xu, Y. Hu, H. Zheng, S. L. Suib and B. Liu, *Appl. Catal., B*, 2018, **238**, 525–532.
17 R. Sandström, G. Hu and T. Wågberg, *ACS Appl. Energy Mater.*, 2018, **1**, 7106–7115.
18 Y. Feng, L. Bu, S. Guo, J. Guo and X. Huang, *Small*, 2016, **12**, 4464–4470.
19 L. Huang, X. Zhang, Y. Han, Q. Wang, Y. Fang and S. Dong, *Chem. Mater.*, 2017, **29**, 4557–4562.
20 K. Zhang, H. Xu, B. Yan, J. Wang, Z. Gu and Y. Du, *Appl. Surf. Sci.*, 2017, **425**, 77–82.
21 M. L. N. Thi, T. H. Tran, P. D. H. Anh, H. T. Nhac-Vu and Q. B. Bui, *J. Alloys Compd.*, 2019, **797**, 314–324.
22 L. Ning, X. Liu, M. Deng, Z. Huang, A. Zhu, Q. Zhang and Q. Liu, *Electrochim. Acta*, 2019, **297**, 206–214.
23 Z. Xi, J. Li, D. Su, M. Muzzio, C. Yu, Q. Li and S. Sun, *J. Am. Chem. Soc.*, 2017, **139**, 15191–15196.
24 X. Y. Ma, Y. Chen, H. Wang, Q. X. Li, W. F. Lin and W. B. Cai, *Chem. Commun.*, 2018, **54**, 2562–2565.
25 C. Peng, Y. Hu, M. Liu and Y. Zheng, *J. Power Sources*, 2015, **278**, 69–75.
26 M. Liu, Y. Lu and W. Chen, *Adv. Funct. Mater.*, 2013, **23**, 1289–1296.
27 X. Guo, H. Shang, J. Guo, H. Xu and Y. Du, *Appl. Surf. Sci.*, 2019, **481**, 1532–1537.
28 D. Chen, P. Sun, H. Liu and J. Yang, *J. Mater. Chem. A*, 2017, **5**, 4421–4429.
29 S. Luo, M. Tang, X. Wu, Y. Ou, Z. Wang, N. Jian, X. Li, Y. Lin, Y. Yan, J. Huang, H. Zhang and D. Yang, *CrystEngComm*, 2019, **21**, 290–296.
30 J. Hu, X. F. Wu, Q. F. Zhang, M. Y. Gao, H. F. Qiu, K. K. Huang, S. H. Feng, T. T. Wang, Y. Yang, Z. L. Liu and B. Zhao, *Langmuir*, 2018, **34**, 2685–2691.
31 A. Mahajan, S. Banik, D. Majumdar and S. K. Bhattacharya, *ACS Omega*, 2019, **4**, 4658–4670.
32 Q. Yan, L. Cao, H. Dong, Z. Tan, Q. Liu, W. Zhan, P. Zhao, Y. Li, Y. Liu and Y. Dong, *Anal. Chim. Acta*, 2019, **1069**, 117–125.
33 C. Tang, N. Zhang, Y. Ji, Q. Shao, Y. Li, X. Xiao and X. Huang, *Nano Lett.*, 2019, **19**, 1336–1342.
34 Q. Shi, C. Zhu, C. Bi, H. Xia, M. H. Engelhard, D. Du and Y. Lin, *J. Mater. Chem. A*, 2017, **5**, 23952–23959.
35 R. Jana, U. Subbarao and S. C. Peter, *J. Power Sources*, 2016, **301**, 160–169.
36 H. Xu, P. Song, C. Fernandez, J. Wang, M. Zhu, Y. Shiraishi and Y. Du, *ACS Appl. Mater. Interfaces*, 2018, **10**, 12659–12665.
37 T. Asset, A. Serov, M. Padilla, A. J. Roy, I. Matanovic, M. Chatenet, F. Maillard and P. Atanassov, *Electrocatalysis*, 2018, **9**, 480.
38 Z. Li, B. Gu, Z. Jiang, X. Zhao, W. Zhu, Y. Zhang, T. Li, X. Du and J. Wu, *J. Taiwan Inst. Chem. Eng.*, 2019, **95**, 131–138.
39 B. F. Machado, A. Marchionni, R. R. Bacsa, M. Bellini, J. Beausoleil, W. Oberhauser, F. Vizza and P. Serp, *J. Energy Chem.*, 2013, **22**, 296–304.
40 S. Sankar, N. Watanabe, G. M. Anilkumar, B. N. Nair, S. G. Sivakamiammal, T. Tamaki and T. Yamaguchi, *Catal. Sci. Technol.*, 2019, **9**, 493–501.
41 X. X. Cui, Y. L. Li, M. Y. Zhao, Y. S. Xu, L. L. Chen, S. G. Yang and Y. Wang, *Nano Res.*, 2019, **12**, 351–356.
42 S. S. Li, Y. Y. Hu, J. J. Feng, Z. Y. Lv, J. R. Chen and A. J. Wang, *Int. J. Hydrogen Energy*, 2014, **39**, 3730–3738.
43 W. Su, R. Sun, F. Ren, Y. Yao, Z. Fei, H. Wang, Z. Liu, R. Xing and Y. Du, *Appl. Surf. Sci.*, 2019, **491**, 735–741.
44 J. Hu, X. F. Wu, Q. F. Zhang, M. Y. Gao, H. F. Qiu, K. K. Huang, S. H. Feng, Y. Yang, Z. L. Liu and B. Zhao, *Electrochem. Commun.*, 2017, **83**, 56–60.